Nuclear Engineering and Technology 55 (2023) 1300–1309

Contents lists available at ScienceDirect

Nuclear Engineering and Technology

journal homepage: www.elsevier.com/locate/net

Original Article

Phase analysis of simulated nuclear fuel debris synthesized using UO_2, Zr, and stainless steel and leaching behavior of the fission products and matrix elements

Ryutaro Tonna [a], Takayuki Sasaki [a, *], Yuji Kodama [a], Taishi Kobayashi [a], Daisuke Akiyama [b], Akira Kirishima [b], Nobuaki Sato [b], Yuta Kumagai [c], Ryoji Kusaka [c], Masayuki Watanabe [c]

[a] Department of Nuclear Engineering, Kyoto University, Kyoto Daigaku-Katsura, Nishikyo, Kyoto, 615-8540, Japan
[b] Institute of Multidisciplinary Research for Advanced Materials (IMRAM), Tohoku University, 1-1 Katahira, 2-chome, Aoba-ku, Sendai, 980-8577, Japan
[c] Nuclear Science and Engineering Center, Japan Atomic Energy Agency (JAEA), Tokai, Ibaraki, 319-1195, Japan

ARTICLE INFO

Article history:
Received 30 July 2022
Received in revised form
30 November 2022
Accepted 14 December 2022
Available online 14 December 2022

Keywords:
Fukushima Daiichi nuclear power station
Simulated fuel debris
Alloy
Fission product
Static leaching

ABSTRACT

Simulated debris was synthesized using UO_2, Zr, and stainless steel and a heat treatment method under inert or oxidizing conditions. The primary U solid phase of the debris synthesized at 1473 K under inert conditions was UO_2, whereas a (U, Zr)O_2 solid solution formed at 1873 K. Under oxidizing conditions, a mixture of U_3O_8 and (Fe, Cr)UO_4 phases formed at 1473 K, whereas a (U, Zr)O_{2+x} solid solution formed at 1873 K. The leaching behavior of the fission products from the simulated debris was evaluated using two methods: the irradiation method, for which fission products were produced via neutron irradiation, and the doping method, for which trace amounts of non-radioactive elements were doped into the debris. The dissolution behavior of U depended on the properties of the debris and aqueous solution for immersion. Cs, Sr, and Ba leached out regardless of the primary solid phases. The leaching of high-valence Eu and Ru ions was suppressed, possibly owing to their solid-solution reaction with or incorporation into the uranium compounds of the simulated debris.

1. Introduction

During the severe accident at the Tokyo Electric Power Company Fukushima Daiichi Nuclear Power Station (1F) Japan, the fuel materials in the molten core reacted with the zircaloy cladding (Zry) and core structure materials, such as stainless steel (SUS), and formed fuel debris under the high-temperature conditions in the pressure vessel [1]. Thousands of tons of seawater were injected into the reactor to cool the core. Although the pressure and containment vessels of the boiling-water reactor were filled with N_2 gas, the oxygen potential increased in unit 3 because of the influx of air caused by the damage to the reactor building [2]. The properties of fuel debris depend on the composition of the atmosphere and temperature at the time of its formation. In previous studies, various simulated debris were synthesized using an alloy phase (e.g., Zry and SUS) in a wide range of temperatures and under various atmospheres assumed to occur during accidents [3–10]. Moreover, the chemical properties of the simulated debris were investigated. Although UO_2 fuel is stable under inert gas conditions, it was oxidized to higher oxides, such as UO_{2+x} and U_3O_8, in the presence of O_2. Assuming that ZrO_2 was formed via the oxidation of Zry, a (U, Zr)O_2 solid solution formed at various heating temperatures and using different melting tests [3–5]. The iron and chromium oxides in SUS yielded $FeUO_4$ and (Fe, Cr)UO_4 in addition to uranium and iron oxides [6,7]. Recently, the simulated debris generated using a complex U–Zr–Fe–O system has been investigated. Under an oxidizing atmosphere, $FeUO_4$ and Zr(IV)-and-Fe(II)-containing UO_2 solid-solution phases were formed in addition to uranium, iron, and zirconium oxides [7–10].

The fuel debris from 1F has been stored under cooling water for over a decade [11,12]. Therefore, radionuclides have been leaching from the debris surface, and the debris has been aging. Evaluating the chemical properties of fuel debris and its leaching behavior is critical for the safe retrieval, storage, treatment, and final disposal

* Corresponding author. Department of Nuclear Engineering, Kyoto University, Kyoto Daigaku-Katsura, Nishikyo, Kyoto, 615-8540, Japan.
E-mail address: sasaki.takayuki.2a@kyoto-u.ac.jp (T. Sasaki).

https://doi.org/10.1016/j.net.2022.12.017

of the 1F debris. However, the 1F debris has not been sampled or directly investigated because of the high levels of radiation and heat it generated; hence, information about it is scarce. Therefore, basic investigations using simulated debris are needed for future actual debris analysis [3,10].

The leaching behavior of radionuclides has been thoroughly investigated by immersing simulated debris samples in aqueous solutions. In previous studies, the short-half-life fission products (FPs) of Zr, Ru, I, Cs, Ba, Ce, and Np were added to the simulated debris of UO_2 and a UO_2–ZrO_2 solid solution via thermal neutron irradiation in a research reactor [3,13]. In addition, the behavior of the FPs during dissolution in seawater was investigated by measuring the radioactivity of the FPs using a Ge semiconductor detector. During leaching tests, the U(VI) species in the oxidized U_3O_8 dissolved easier than the U(IV) species in the UO_2–ZrO_2 solid solution. The mono- and divalent ions, such as Cs^+, I^-, and Ba^{2+}, leached preferentially over U from the UO_2–ZrO_2 solid solution and U_3O_8. However, the leaching of polyvalent Zr and Ce ions was insignificant, and the apparent concentration of Zr was higher than the estimated solubility of Zr owing to the formation of colloids. The actinide tracers ^{237}Np, ^{236}Pu, and ^{241}Am were doped into the UO_2–ZrO_2 solid solution or Zr–Fe alloy before the heat treatment step of the synthesis process, and it was determined that their leaching ratios in seawater were significantly low [10,14,15]. Therefore, it was concluded that the Zr species in the UO_2 crystal structure suppressed the leaching of FPs and actinides owing to the formation of a stable UO_2–ZrO_2 solid solution. However, the dissolution behavior of FPs in simulated fuel debris fabricated using metals or alloys, such as Zr and SUS, has not been investigated systematically.

In this study, simulated debris samples were fabricated using UO_2, Zr, and SUS. Thereafter, the leaching of FPs and U from the simulated debris samples was investigated using a similar method in our previous studies on UO_2 and UO_2–ZrO_2 solid-solution systems [13]. Neutron irradiation and doping methods were used to fabricate debris samples and add various types of nuclides to them. The trace amount of radioactive FPs in simulated debris fabricated using the neutron irradiation method typically decays within a year. In contrast, the long-half-life or non-radioactive elements (cold FPs) in simulated debris fabricated using the doping method can be detected using inductively coupled plasma–mass spectrometry (ICP–MS) even after prolonged immersion.

2. Experimental

2.1. Preparation of simulated debris

2.1.1. Materials

UO_2 was prepared by heating U_3O_8 at 1273 K under an Ar + 4% H_2 atmosphere for 4 h. The formation of UO_2 was confirmed using powder X-ray diffraction (XRD) measurements. SUS 304 powder (>99%, <100 mesh), comprising 68.77% Fe, 18.71% Cr, and 11.09% Ni, was purchased from Nilaco. Zr (95.0%), ZrO_2 (98.0%), Cs_2CO_3(95.0%), $SrCO_3$ (99.99%), and Eu_2O_3 (99.9%) were purchased from FUJIFILM Wako Pure Chemicals.

The simulated debris samples are denoted using six-digit symbols that indicate the experimental conditions during synthesis and the aqueous solutions they were immersed in (Table 1). The compositions of the mixed materials in the simulated debris fabricated in this study were set to U:Zr:(Fe + Cr + Ni in SUS 304) = 1:1:1, U:Zr (or ZrO_2) = 1:1, and U:(Fe + Cr + Ni in SUS 304) = 1:1 (molar ratios) to distinguish the phase changes. For the doping method, the atomic ratios of Cs-, Sr-, and Eu-to-U were 0.57%, 1.6%, 0.53 × 10^{-2}%, respectively, for the UO_2–SUS–Zr samples (DAG and DAO) and 5.4, 6.0, and 5.0 × 10^{-2}%, respectively, for the other system samples (DXO, DXG, DSG, and DZG).

2.1.2. Irradiation method

Natural uranium dioxide (^{235}U = 0.72%) was used for the samples synthesized by the irradiation method. UO_2 was mixed with ZrO_2, Zr, and SUS powders, and the mixtures were ground for 20 min using an agate mortar. After the XRD pattern of the mixture was obtained, a quartz or alumina boat containing the mixture was placed in the center of a quartz or alumina reaction tube. The reaction tube was evacuated and then refilled with ultrapure Ar (denoted as 1 ppm O_2), or Ar + 4% H_2, which were used to achieve various oxygen potentials. Next, each sample was heated for the designated time at 1473 and 1873 K (ramping rate of approximately 10 K min^{-1}). Thereafter, the samples were cooled to 873 K (ramping rate of approximately 7 K min^{-1}), and the furnace was cooled to room temperature. The heated sample was grounded in an agate mortar, and a solid-state analysis was conducted. In some samples, it partially reacted with the alumina boat during heating and was lost. Finally, the samples were irradiated with thermal neutrons using the pneumatic transferring system (Pn-2) of the Kyoto University Reactor, as described previously [3,16]. The nuclides in the samples were generated primarily via the fission reaction of ^{235}U. To perform an inventory evaluation of the FPs, the gamma-ray spectra of the neutron-irradiated samples were obtained using a Ge semiconductor detector (GC4020, Canberra) prior to the leaching tests.

2.1.3. Doping method

UO_2 was mixed with ZrO_2, Zr, and SUS powders using a similar method described in Section 2.1.2. Before the heating treatment, three non-radioactive reagents: Cs_2CO_3, $SrCO_3$, and Eu_2O_3, served as cold FPs of mono-, di-, and trivalent ions, respectively, were added to the mixture. The heating conditions were the same as those used for the irradiation method. In addition to Ar (denoted as 1 ppm O_2) and Ar + 4% H_2 atmosphere conditions, the mixture was heated under Ar + 2% O_2 atmosphere. For some UO_2-Zr-SUS samples, the atmospheric conditions were controlled to Ar + 2% O_2 under constant temperature heating conditions, while 1 ppm O_2 atmosphere conditions were applied for the heating up and down processes.

2.2. Analysis of simulated debris

The XRD patterns of the prepared samples were obtained using a SmartLab SE (Rigaku) instrument with Ni-filtered Cu Kα radiation, which was operated at 50 kV and 40 mA. The XRD patterns of the samples were collected at a scan rate of 2° min^{-1} in the 2θ range of 5°–80° using a step size of 0.01°. The phases of the products were determined by matching the observed patterns with those in the Crystallography Open Database [17]. The lattice parameters and weight fraction of the compounds were calculated using Rietveld analysis [18]. Especially in the case of complex compositions such as mixtures of samples, Rietveld analysis provides semi-quantitative information but could be referenced to evaluate trends in changes in solid phase conditions due to heating conditions and other factors. The microstructure and elemental composition of several samples were evaluated using a scanning electron microscopy (SEM; JCM-6000, NeoScope, JEOL) instrument equipped with energy-dispersive X-ray spectroscopy (EDX; EX-37001, JEOL) apparatus. The accelerating voltage was set to 15 kV. Prior to the SEM–EDX experiments, the samples were adhered to carbon tape and coated with Pt–Pd using a magnetron sputter (MSP-1S, Vacuum Device) for 1 min.

Table 1
Six-digit symbols of the simulated debris samples indicating the synthesis conditions and immersion solutions.

1	2	3	4	5	6
FPs	Mixture	Atmosphere[a]	Heating temperature	Heating time (x)[b]	Immersion solution
D doping	X none	O Ar–2% O_2	L 1473 K	0	S seawater[c]
I irradiation	A Zr + SUS	G 1 ppm O_2	H 1873 K	1 1 h	N $NaClO_4$
_	Z ZrO_2	R Ar–4% H_2	–	2 2 h	–
_	S SUS	–	–	4 4 h	–
_	–	–	–	8 8 h	–

FPs, fission products; SUS, stainless steel.
[a] An Ar atmosphere was used during the heating and cooling.
[b] (1 + 1) h for 2 h, (1 + 1 + 2) h for 4 h, and (1 + 1 + 2 + 4) for 8 h.
[c] Daigo's artificial seawater SP.

2.3. Static leaching test of the simulated debris

For the leaching test, the solid-to-liquid ratio was set to 1 g dm^{-3}. Each simulated debris sample was added to a polypropylene tube filled with a 0.1 M $NaClO_4$ solution containing a pH buffer (10 mM PIPES, Dojindo) or Daigo's artificial seawater SP (Nihon Pharmaceutical) [19], which is typically used as a medium for marine microalgae. The tubes were shaken slowly using a shaker (BR-43FL-MR, Taitec) under atmospheric conditions at 298 K. The primary anionic components of the seawater were Cl^-, CO_3^{2-}, and SO_4^{2-} ions, and their initial concentrations were 0.47 M, 2.85 mM, and 36 mM, respectively. The composition of Daigo's artificial seawater SP is summarized in Table S1. For simplicity, for the thermodynamic simulation of uranium solubility, the CO_3^{2-} ions in $NaClO_4$ and Daigo's artificial seawater SP were assumed to be 0.1 and 0.9 mM, respectively, considering the situation of water equilibrium with air. Therefore, the partial pressure of CO_2 in the atmosphere was set to 3.9×10^{-4} atm, and the thermodynamic constants used to calculate the concentration of CO_3^{2-} ions at equilibrium are summarized in Table S2.

After shaking, the pH of each mixture was measured using a combination glass electrode (9615S-10D, Horiba), and the redox potential (Eh) was measured using a Pt oxidation-reduction potential electrode (9300-10D, Horiba), which was filled with a mixture of 3.6 M NaCl and 0.4 M $NaClO_4$. A small amount of the supernatant was filtered using a 0.45 μm pore polytetrafluoroethylene (PTFE) membrane (Dismic, Advantec), and the concentrations of the leached nuclides were determined. Four additional ultrafiltration filters with different pore sizes in the range of 3–100 kDa were used to filter the simulated UO_2–Zr–SUS debris samples prepared using the doping method to confirm that the leached radionuclides formed colloids.

For the irradiation method, 1- and 10-mL aliquots of the filtrate samples were used. The 1 mL aliquots were used to measure the concentrations of U, Fe, Cr, Ni, and Zr leached using an ICP–MS (ICPMS-2030, Shimazu) instrument. 0.1 mL HNO_3 was added to each 10 mL aliquot, and the mixtures were gently evaporated at 365 K to obtain solidified point-like sources at the bottom of the sample tubes for gamma-ray measurement. The cumulative gamma radioactivity of the nuclides was determined by considering the background reduction and decay correction in accordance with a previously reported method [13]. The leached concentration of nuclide (M) at a given immersion time would depend on the surface condition of the solid sample. In this study, the dissolution behavior was evaluated by the leaching ratio of the concentration of M to the initial inventory since there are no details, such as the specific surface area and the elemental distribution on the solid surface. The leaching ratio (r_M) was calculated as follows:

$$r_M = \frac{A_{f,M} \exp\left(\frac{T_{1/2,M}}{t \ln 2}\right)}{A_{i,M}}, \quad (1a)$$

where $A_{i,M}$ is the initial radioactivity (Bq) of nuclide M in the simulated debris sample, $A_{f,M}$ is the radioactivity (Bq) in the filtrate after the leaching period (t), and $T_{1/2,M}$ is the decay half-life of nuclide M (day).

For the doping method, 1 mL of the supernatant was filtered, and the concentrations of the cold FPs (Cs, Sr, Eu) and matrix elements (U, Fe, Cr, Ni, and Zr) were measured using ICP–MS. The r_M values of the nuclides were calculated as follows:

$$r_M = \frac{C_{f,M} V}{M_{i,M}}, \quad (1b)$$

where $C_{f,M}$ is the molar concentration of nuclide M in the filtrate (mol dm^{-3}), V is the volume of the filtrate (dm^3), and $M_{i,M}$ is the initial concentration of nuclide M (mol). During the high-temperature heat treatment of the samples, fractions of the amounts of cold FPs were lost via volatilization. Therefore, the loss ratio (v_M) was determined using Eq. (2), and $M_{i,M}$, was corrected using v_M.

$$v_M = 1 - \frac{N_M}{N_{i,M}}, \quad (2)$$

where $N_{i,M}$ and N_M are the ratios of the initial concentration of nuclide M in the cold FPs to that of U before and after heating ($N_{i,M} = M_{i,M}/M_{i,U}$)

To evaluate N_M, 15 mg of the sample was dissolved in hot 60% HNO_3, the amount of each element was measured using ICP–MS, and the results were used to determine N_M [20]. However, the alloy phases added to debris samples can be insoluble. Consequently, the debris was melted by heating it with sodium peroxide as follows. 15 mg simulated debris sample was mixed with 150 mg of sodium peroxide in a Ni crucible and heated at 1023 K under atmospheric conditions for 15 min. After that, double-deionized water and HNO_3 were added to a Ni crucible. The residue was filtered using a 0.45 μm pore PTFE membrane filter, and then the concentrations of U and cold FPs were measured using ICP–MS. The v_M values were evaluated using HNO_3 for the DXRL4, DXOL4, DXRH1 and DXOH1 samples, which contained UO_2, and sodium peroxide for the DSOL4, DAGL1, DAOL1, DAGH1, and DAOH1 samples, which contained Zr or SUS.

3. Results and discussion

3.1. Phase relations

3.1.1. DAGLx (x = 1, 2, 4, 8), and DXRL4 samples

The XRD patterns of the DAGLx (x = 0, 1, 2, 4, 8) samples before and after heat treatment and DXRL4 are shown in Fig. S1 (Supplementary Material). The peaks of UO_2, Zr metal, and Fe metal in SUS were observed in the XRD patterns of the mixed samples before heating, whereas the peaks of Cr and Ni metals, which were minor components of SUS, were not present. The characteristic diffraction peaks of UO_2 did not change significantly even after 8 h of heating under a 1 ppm O_2 atmosphere. The lattice parameter of the UO_2 phase in the DAGL8 sample was calculated to be 5.4707(5) Å using Rietveld analysis, and this value was consistent with the previously reported lattice parameter of 5.4704 Å [21]. These results indicated that UO_2 did not undergo oxidation, and a solid solution comprising Zr and SUS did not form. The characteristic diffraction peaks of UO_2 did not change after 4 h of heating under Ar + 4% H_2 (DXRL4) as well as DAGLx and no oxidation reaction was observed. The diffraction peak of Zr metal in the DAGLx samples was downshifted after 1 h of heating treatment, and the new peaks were assigned to a zirconium-oxygen solid-solution (Zr(O)), such as Zr_3O. Furthermore, the crystallinity of Zr metal powder in the absence of UO_2 and SUS decreased after 1 h of heating at 1473 K under a 1 ppm O_2 atmosphere. However, the diffraction peak of Zr did not downshift (Fig. S2), indicating that Zr(O) did not form via slow oxidation under a 1 ppm O_2 atmosphere but owing to the coexistence of UO_2 and SUS in the samples. In addition, the characteristic peaks of the other Zr alloy phases, namely Fe_2Zr and $FeZr_2$ were observed in the XRD patterns of the DAGLx samples (Fig. S1). The strongest peaks of $FeZr_2$ were observed in DAGLx, but subpeaks were not observed due to small amount of $FeZr_2$ formed. $FeZr_2$ is thermodynamically expected to form during the cooling process [22]. Cr and Ni in stainless steel are expected to form Cr–Zr and Ni–Zr alloy phases thermodynamically, but these phases were not confirmed by XRD due to the tiny amount of Cr–Zr and Ni–Zr alloy phases formed [23,24]. The Rietveld analysis of the DAGLx samples suggested that the weight fraction of Zr(O) decreased with heating time, whereas those of Fe_2Zr and $FeZr_2$ increased with heating time (Fig. 1), indicating that Zr(O) reacted with Fe resulting Fe–Zr alloy.

3.1.2. DAGHx (x = 1, 2, 4, 8), DXGH1, DXRH1, DSGH1, DZGH1, IAGH1, IXGH1, ISGH1, and IZGH1 samples

Several samples with different initial compositions, which were synthesized via heating at 1873 K under a 1 ppm O_2 atmosphere, were analyzed. The XRD patterns of the UO_2 (DXGH1, DXRH1, IXGH1), UO_2–SUS (DSGH1, ISGH1), and UO_2–ZrO_2 (DZGH1, IZGH1) samples are shown in Fig. S3, and those of the UO_2–Zr–SUS (DAGHx (x = 1, 2, 4, 8) and IAGH1) samples are shown in Fig. S4. The peaks of UO_2 in the XRD patterns of the DXGH1, DXRH1, and DSGH1 samples were comparable, suggesting that UO_2 did not undergo significant oxidation at 1873 K under a 1 ppm O_2 and Ar + 4% H_2 atmosphere, and a reaction between UO_2 and Fe and Cr in the SUS did not occur. Conversely, the characteristic peaks of the UO_2 phase in the XRD pattern of DZGH1 upshifted from the initial position owing to the solid-solution reaction of Zr with the UO_2 phase [25]. Solid-solution (U, Zr)O_2 phases were also present in the DAGH1 and IAGH1 samples in addition to the initial UO_2 phase. The relative ratio of UO_2 to the (U, Zr)O_2 phase decreased with increasing heating time, as seen in the results of DAGHx samples. After 8 h of heating, the formation of the (U, Zr)O_2 phase was complete. The positions of the characteristic peaks of the (U, Zr)O_2 phase in the XRD patterns of the samples obtained after 1 and 8 h of heating were the same. The lattice parameter of the (U, Zr)O_2 phase, which was obtained using Rietveld analysis, decreased from 5.4704 Å [21] to 5.3933(9) Å after 1 h of heating. It was almost constant (5.4196(9) Å) after 8 h of heating (Fig. 2). The mole fraction of Zr in the (U, Zr)O_2 phase of the DAGHx samples was calculated using Vegard's law, which stipulates that a linear relationship exists between the lattice parameter of a crystal and the mole ratio of elements in the solid phase. The lattice parameters of UO_2 and cubic ZrO_2 used as reference phases were 5.4704 Å [21] and 5.135 Å [26], respectively. The mole fraction of Zr in the (U, Zr)O_2 phase of the DAGH8 sample was calculated to be 17%, which was slightly higher than the limit of Zr solid solution in the UO_2 phase (13%) [27]. The solid-solution reaction of Fe [10], and the hyper-oxidation of UO_2 [28] also caused a decrease in the lattice parameter of the UO_2 phase; therefore, the solid-solution reaction of Zr and Fe, and the hyper-oxidation of U could have simultaneously occurred during heating at 1873 K under a 1 ppm O_2 atmosphere [28]. Kirishima et al. synthesized a UO_2–SUS–Zr debris by heating a mixture of UO_2, SUS, and Zr at 1873 K under a 1 ppm O_2 atmosphere for 12 h and reported that the solid-solution reaction of Fe with the UO_2 phase causes a decrease in the lattice constant of the UO_2 phase [10]. After heating, the diffraction peak of UO_2 was split into the initial peak of UO_2 and the peak of the (U, Zr)O_{2+x} solid solution. Moreover, the intensities of the initial UO_2 peak and the peak of the (U, Zr)O_{2+x} solid solution decreased and increased, respectively, with heating time (Fig. S4). These findings suggested that a solid solution of Zr occurred at the surface of the grains and leached to the upper limit of Zr solid solution, whereas the formation of Zr solid solution required 8 h to reach the core of the UO2 particle under the heating conditions in this study. In addition to the (U, Zr)O_{2+x} solid solution, a Zr–Fe alloy was formed via heating for 1 h. Upon further heating, the amounts of Zr–Fe alloy and tetragonal ZrO_2 (t-ZrO_2) phases increased. Although monoclinic ZrO_2 (m-ZrO_2) is stable at room temperature, in this study, we considered that ZrO_2 was present as t-ZrO_2 because of the dissolution of U into the ZrO_2 phase [29]. Therefore, it was hypothesized that Zr formed alloys with the Fe in SUS immediately after heating at 1873 K under a 1 ppm O_2 atmosphere. However, the Zr in the Zr–Fe alloy slowly and gradually oxidized to ZrO_2, and then the solid-solution reaction of ZrO_2 with UO_2 would occur. Although the oxygen potential is lower at 1873K than 1473 K, the oxidation reaction of Zr progressed in DAGHx, supposing that the oxygen diffused faster in the solid phase at 1873K than 1473 K. The SEM-EDX image of DAGH1 particles showed that the particle size was almost uniform at several tens of micrometers by mortar grinding. It was also found that U and Zr were distributed in different positions (Fig. S5).

This was consistent with the XRD results, which indicated the presence of UO_2 and t-ZrO_2 in the sample. Segregation of the Sr doped as cold FP was also observed; however, the segregation of Cs and Eu was not observed.

3.1.3. DAOLx (x = 1, 2, 4, 8) samples

The XRD patterns of the DAOLx (x = 1, 2, 4, 8) samples are shown in Fig. S6. The characteristic peaks of UO_2 upshifted slightly after 1 h of heating. After 2 h of heating, the peaks upshifted more significantly, and the characteristic peak of U_3O_8, which formed via the oxidation of UO_2, was distinctly observed in the XRD pattern of the DAOL2 sample. These results indicated that the shift in the peak of UO_2 was caused by the hyper-oxidation of UO_2 and the formation of UO_{2+x} [28]. In addition to U, Fe was also oxidized, and the characteristic peak of Fe_2O_3 was observed in the XRD pattern of DAOL1. The characteristic peaks of the (Fe, Cr)UO_4 phase, which formed via the complexation of UO_2 with the Fe and Cr in SUS, emerged in the XRD pattern of DAOL2 [7]. It was suggested that (Fe, Cr)UO_4 formed in the presence of O_2 via the reaction of U_3O_8 with Cr_2O_3, which yielded $CrUO_4$, followed by the reaction of $CrUO_4$ with Fe_3O_4 at

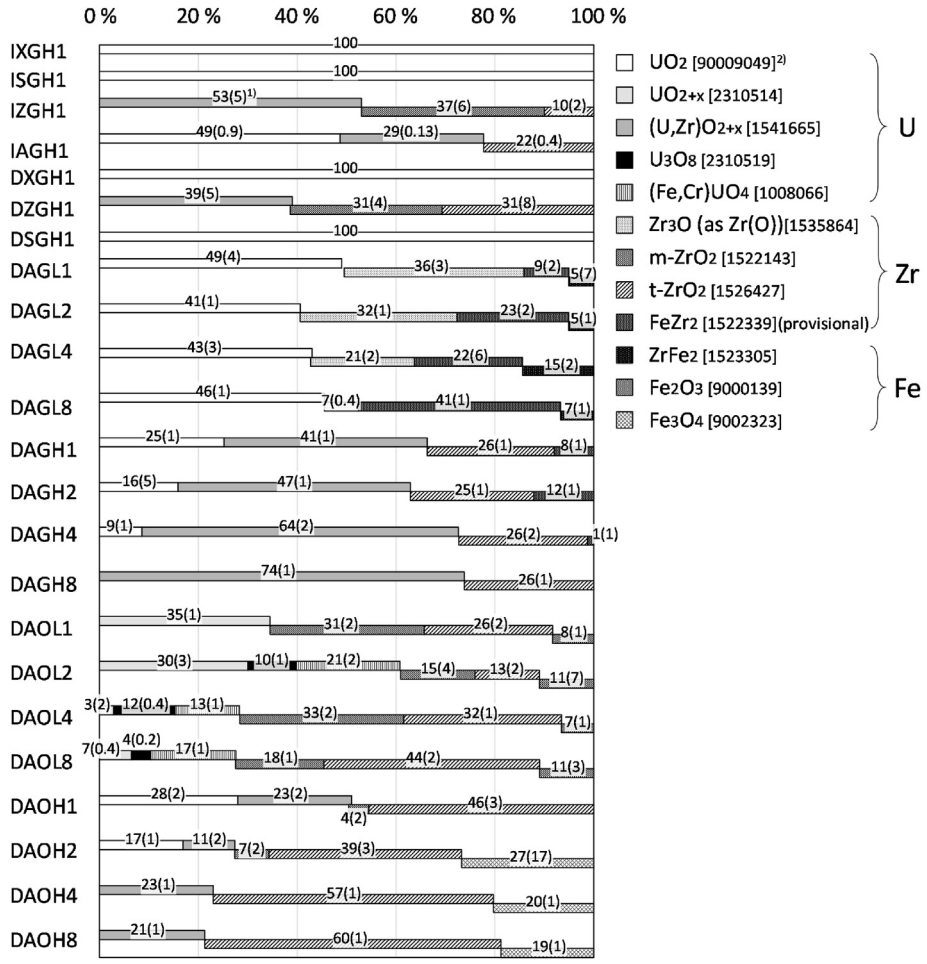

Fig. 1. Weight percentages of the components of the simulated debris estimated using Rietveld analysis. [1)]The values in parentheses represent standard errors. [2)]Crystallography Open Database numbers.

1473 K [7]. Because no characteristic peaks of chromium oxides were observed in the XRD pattern of DAOL2, it was hypothesized that most of the chromium oxides reacted with U_3O_8 to form the (Fe, Cr)UO_4 phase.

Both m-ZrO_2 and t-ZrO_2 were present in the DAOL1 sample. Because the characteristic peak of Zr metal was not observed in the XRD pattern of DAOL1, it was concluded that the oxidation of Zr proceeded to completion. Furthermore, the intensity of the diffraction peak of m-ZrO_2 decreased gradually, whereas that of the diffraction peak of t-ZrO_2 increased gradually as the heating time was increased to 8 h. These results indicated that Zr was oxidized to m-ZrO_2 and then underwent a solid-solution reaction with U to form t-(Zr, U)O_2, which was stable even at room temperature, as shown in Fig. 1 [29].

3.1.4. *DAOHx (x = 1, 2, 4, 8) samples*

The UO_2 peaks in the XRD patterns of the DAOH1 and DAOH2 samples were slightly upshifted; moreover, the shift in the position of the UO_2 peak in the XRD pattern of DAOH4 indicated the formation of a UO_2–ZrO_2 solid solution (Fig. S7). This peak has been assigned to the (U, Zr)O_2 phase in a previous study, in which UO_2 and m-ZrO_2 mixtures were heated at 1873 K under a 2% O_2 atmosphere for 1 h and heated and cooled under a 1 ppm O_2 atmosphere [30]. The lattice parameter of the UO_2–ZrO_2 solid solution in the DAOH8 sample was 5.3020(5) Å, which was smaller than that of the UO_2–ZrO_2 solid solution in the DAGH8 sample (5.4196(9) Å), for which the molar fraction of Zr in UO_2 would have reached to the solid solution limit at room temperature, 13% [27]. These results indicated that the UO_2 phase underwent an oxidation reaction, followed by a solid-solution reaction with Fe in addition to the solid-solution reaction with Zr [10,28]. No other U phases, such as U_3O_8 and (Fe, Cr)UO_4, were formed in the DAOHx samples; however, they formed in the DAOLx samples. In addition to the solid solution of Zr in the UO_2 phase, t-ZrO_2 and m-ZrO_2 phases were formed after 1 h of heating. No characteristic peaks of Zr metal were present in the XRD pattern of the samples in the DAO-series, suggesting that the oxidation of Zr proceeded to completion. Upon further heating, the characteristic peak of m-ZrO_2 disappeared, and only the t-ZrO_2 peak was observed. These findings indicated that metallic Zr was oxidized to m-ZrO_2 upon heating at 1873 K under a 2% O_2 atmosphere, and then m-ZrO_2 underwent a solid-solution reaction with U to form t-(Zr, U)O_2, which was stable at room temperature [27]. The characteristic peaks of magnetite (Fe_3O_4) as a Fe solid phase, were observed in the XRD patterns of the DAOHx samples, whereas the characteristic peaks of alloy phases, such as Fe_2Zr and $FeZr_2$, were not present in the XRD patterns of the DAOHx samples. These findings indicated that oxidation reactions predominated over alloy phase formation under a 2% O_2 atmosphere at 1873 K.

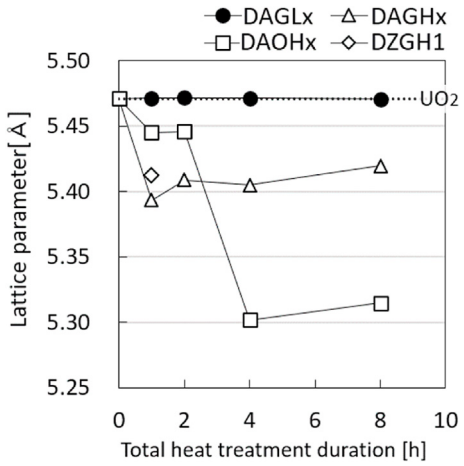

Fig. 2. Relationship between the lattice parameters of the cubic UO_2 phase of the simulated debris and total duration of the heat treatment.

3.2. Loss of radionuclide inventory of the samples fabricated using the doping method

The loss ratios of the doped Cs, Sr, and Eu of the samples fabricated using the doping method were evaluated. The ratios were independent of the heating atmosphere but depended on temperature. The loss ratios of the samples heated at 1873 K were higher than those heated at 1473 K. No significant heating time dependence on the loss ratios was observed. The average values of the loss ratios of Cs, Sr, and Eu for the DAGLx and DAOLx (x = 1, 2, 4, 8) samples were 97%, 29%, and 24%, respectively, and 99.86%, 72%, and 58% for the DAGHx and DAOHx (x = 1, 2, 4, 8) samples. These data suggested that the loss of radionuclides decreased as follows: Cs ≫ Sr > Eu, and Cs and Sr loss occurred primarily via volatilization. Eu behaved differently because Eu_2O_3 could have formed and absorbed on the surface of the alumina boat. Therefore, the loss ratios of Cs, Sr, and Eu were used to correct the cold FP inventories of the samples in the DA-series. In addition, the loss ratios of Cs, Sr, and Eu of the samples in the DX-series were determined. The average loss ratios of Cs, Sr, and Eu of the DXRL4 and DXOL4 samples were 87%, 44%, and 0%, respectively, and those of the DXRH1 and DXOH1 samples were 99.4%, 78%, and 45%, respectively. The loss ratios of Cs, Sr, and Eu of the samples in the DS- and DZ-series were not determined. Therefore, the loss ratios of Cs, Sr, Eu for the DSGH1 and DZGH1 samples were assumed to be the same as those in the DX-series, which were prepared using the same initial Cs-, Sr-, and Eu-to-U atomic ratios.

3.3. Leaching behavior of simulated debris

3.3.1. pH and Eh values

The initial pH values of Daigo's artificial seawater SP and the 0.1 M $NaClO_4$ solution before the immersion tests were 8 and 7, respectively. The Eh (*V* vs. normal hydrogen electrode) values of Daigo's artificial seawater SP and the 0.1 M $NaClO_4$ solution revealed that natural oxidizing conditions occurred at approximately 482 mV (pH 7) and 365 mV (pH 8), respectively. The pH and Eh values of the solutions did not change significantly after six months of leaching.

3.3.2. Colloid formation

The DAGL8, DAGH8, and DAOL8 samples were used to analyze the colloid-formation ability of the nuclides in filtrates. The primary U-containing phases of the DAGL8, DAGH8, and DAOL8 samples were UO_2, (U, Zr)O_2, and (Fe, Cr)UO_4, respectively. No colloids of U and cold FPs (Cs, Sr, Eu) were observed in the filtrates of the seawater and $NaClO_4$ solutions. These results agreed with those reported for UO_2 and (U, Zr)O_2 systems fabricated using the irradiation method [13].

3.3.3. U leaching

The time evolution of the U leaching ratio (r_U) is shown in Fig. 3, where log r_U = 0 indicates complete dissolution. The r_U of samples immersed in $NaClO_4$ solution was approximately constant over one year of leaching, independent of the heating condition, suggesting that a steady state was reached. The predominant U phase of the DAGLx samples was UO_2, and an Fe–Zr metal phase was also

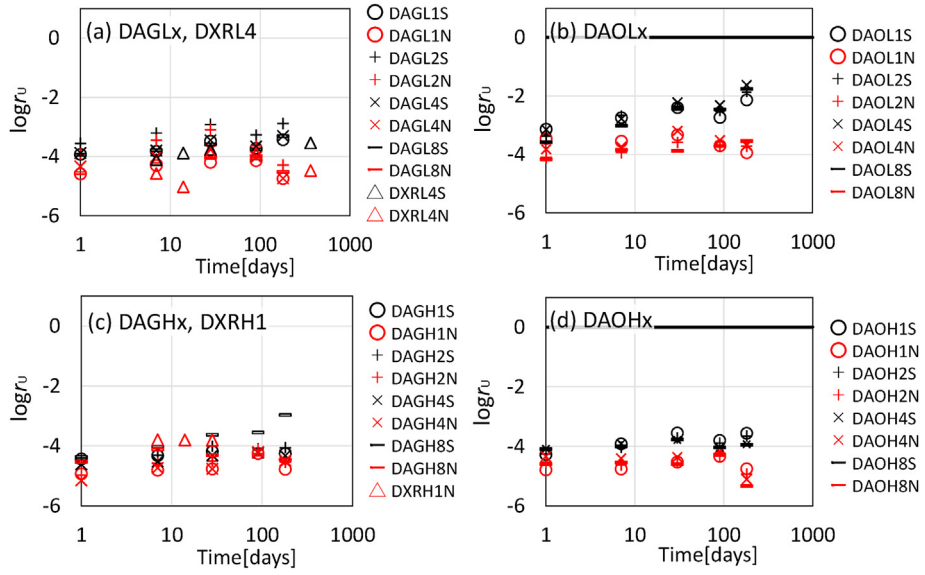

Fig. 3. Time evolution of the leaching ratio of uranium (r_U) for the UO_2 and the UO_2–Zr–SUS samples. The black and red points represent the r_U values in the seawater and $NaClO_4$ solution systems. Samples heated at (a) 1473 K under a 1 ppm O_2 atmosphere (DAGLx, x = 1, 2, 4, 8) and Ar + 4% H_2 atmosphere (DXRL4), (b) 1473 K under a 2% O_2 atmosphere (DAOLx, x = 1, 2, 4, 8), (c) 1873 K under a 1 ppm O_2 atmosphere (DAGHx, x = 1, 2, 4, 8) and Ar + 4% H_2 atmosphere (DXRH1), and (d) at 1873 K under a 2% O_2 atmosphere (DAOHx, x = 1, 2, 4, 8). (For interpretation of the references to colour in this figure legend, the reader is referred to the Web version of this article.)

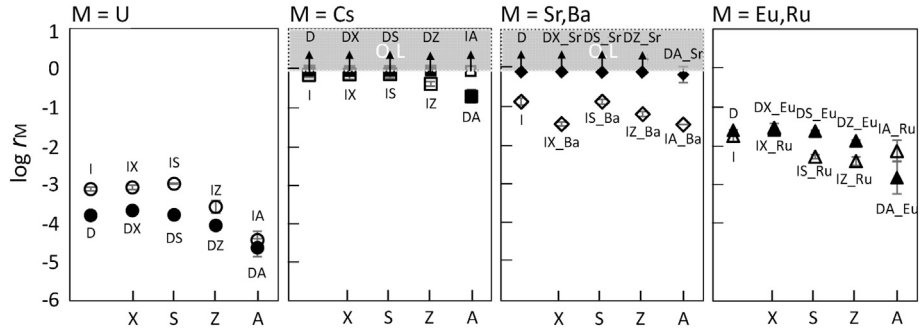

Fig. 4. Average leaching ratios of U and the FPs of the samples heated at 1873 K under a 1 ppm O_2 atmosphere for 1 h (D*GH1 and I*GH1, * = X, S, Z, A) for up to six months after immersion in $NaClO_4$ solution. The solid and open symbols indicate samples fabricated using doping and irradiation methods. The results of the samples heated at 1873 K under an Ar + 4% H_2 atmosphere for 1 h (DXRH1 and IXRH1) are shown in the leftmost column for each figure. The arrow represents the limit of quantification of the mass spectrometer.

present. The log r_U values of the DAGLx samples in the $NaClO_4$ solution (Fig. 3a) were low; they ranged between −3.5. The r_U values of the DAGLx samples were comparable to those of a UO_2 sample heated at 1473 K under reducing conditions [16]. Moreover, the time evolution of the log r_U values of the DAOLx samples comprising mixtures of U_3O_8 and (Fe, Cr)UO_4 (Fig. 3b) was similar to that of the DAGLx samples; however, the log r_U values of the DAOLx samples were slightly higher (in the range of −3 to −4) than those of the DAGLx samples. In a previous study, U dissolution was promoted in samples containing U_3O_8 formed via the oxidation of UO_2 in the UO_2–SUS system during heat treatment [13]. Therefore, the r_U values of the DAOLx samples were consistent with that of U_3O_8 [16], suggesting that the higher r_U values of the DAOLx samples were attributed to the dissolution of soluble U_3O_8. However, the dissolution of the (Fe, Cr)UO_4 phase in the DAOLx samples has not been fully investigated. The r_U values of the DAOLx samples did not depend on heating time. In other words, the r_U values of the DAOLx samples did not depend of the ratio of U_3O_8-to-$FeUO_4$, suggesting that the apparent r_U value or dissolution rate of (Fe, Cr)UO_4 should be lower than that of U_3O_8.

The r_U values of the DAGLx and DAOLx samples immersed in seawater were larger than those of the DAGLx and DAOLx samples immersed in $NaClO_4$, suggesting that the dissolution of U from the solid phase was promoted by the anionic ligands in seawater [13]. The *r*U values of the DAOLx samples (Fig. 3b), which contained a highly oxidized U phase, such as U_3O_8, immersed in seawater were higher than those of the corresponding DAGLx samples (Fig. 3a). The r_U values of the DAGHx (Fig. 3c) and DAOHx samples (Fig. 3d), for which the primary U phases were (U, Zr)O_2 and UO_{2+x}, immersed in $NaClO_4$, were nearly constant over one year. These results were lower (in the range of −4 to−5.5) than those of the DAGLx samples (Fig. 3a). These low r_U values of the DAGHx and DAOHx samples were ascribed to the formation of a (U, Zr)O_{2+x} solid solution because it has been previously reported that the presence of Zr in UO_2 solid solutions suppressed nuclei dissolution [14]. Furthermore, the r_U values of the samples immersed in seawater were not significantly higher than those immersed in $NaClO_4$ for DAGHx except for DAGH8. It was inferred that trace amounts of a soluble U solid phase, which could not be detected via XRD measurements, were present in DAGH8. Further experimental analysis should be performed, especially of the surfaces of simulated debris samples, to elucidate these findings.

Fig. 4 shows the average r_U values of the D*GH1 and I*GH1 (* = X, S, Z, and A) samples and DXRH1 and IXRH1 samples after immersion in $NaClO_4$ solution up to six months. The primary U phase of the samples in the DXR-, DXG- and DSG-series was UO_2, whereas that of the samples in the DZ-series was (U, Zr)O_2 (Fig. 1). These results seemed satisfactory because the r_U value of (U, Zr)O_2 was lower than that of UO_2 (Fig. 3). However, the r_U values of the samples in the DA-series comprising mixtures of UO_2 and (U, Zr)O_2 (Fig. 1) were lower than those of the samples in the DZ-series comprising (U, Zr)O_2. As described in Section 3.1.2, a fraction of the added Zr metal powder was gradually oxidized to ZrO_2 and then dissolved into the UO_2 phase of the simulated debris. The water-insoluble Zr(IV) species in the UO_2- phase-containing compounds suppressed the dissolution of U. In addition to Zr, Fe also formed a solid solution with the UO_2 matrix, stabilizing the UO_2 phase of the UO_2–SUS–Zr system [10]. Therefore, the r_U values of the samples in the DA-series were lower than those in the DZ-series because of the presence of the Fe solid solution in the UO_2 phase. However, the presence of a Fe solid solution was not observed in the XRD patterns of the samples in the DA-series.

The solubility of U was evaluated using thermodynamic simulation, and the results were compared with the experimentally determined concentration. Under atmospheric conditions, uranyl ions were predominant, and a secondary mineral comprising U^{6+} ions such as UO_2CO_3(s), $Na_2U_2O_7$, bequerelite ($CaU_6O_{19}\cdot 11H_2O$), or metashoepite ($(UO_2)(OH)_2\cdot H_2O$), was assumed to be the solubility-limiting solid phase. Considering a representative set of experimental conditions, the following solution conditions were adopted: pH = 7, Eh = 482 mV, $\log[CO_3^{2-}] = -6.85$ for the $NaClO_4$ solution and pH = 8, Eh = 365 mV, and $\log[CO_3^{2-}] = -4.85$ for the simulated seawater (Fig. 3). Some anions that strongly coordinate with U can change the apparent solubility of U [31]. Therefore, hydroxide and carbonate species were considered for the $NaClO_4$ solution; sulfate species were also considered for the artificial seawater system. Using the specific ion interaction theory [31], the thermodynamic constants of the carbonate and hydroxide complexes listed in Table S3 were corrected to those under a given ionic strength, *I*, condition. In addition to the ion product ($pK_w = -13.77$) [32], the following ion interaction coefficients were used: H^+ (0.12) for the ClO_4^- and Cl^- systems and OH^- (0.04), CO_3^{2-} (−0.08), and HCO_3^- (0) for the Na^+ system [33]. The standard potential (E^0) of U(VI)–U(IV) is +0.2673 V [34]. Other thermodynamic constants are listed in Table S3.

Fig. 5 shows the thermodynamic simulation of the solubility of U and the experimental plots of DAGL1, DAOL1, DAGH1, and DAOH1 after six months of leaching. The logarithms of the solubility of U in the $NaClO_4$ solution and seawater systems were −6.28 and −3.52, respectively. Uranyl carbonate species were predominant in the neutral pH region for both systems. The carbonate concentration of artificial seawater was higher than that of the $NaClO_4$ solution; therefore, the apparent solubility of U in artificial seawater was two orders of magnitude higher than that in the $NaClO_4$ solution. The uranyl sulfate species became predominant only at pH < 6 in the seawater system, suggesting that the contribution of SO_4^{2-} ions to

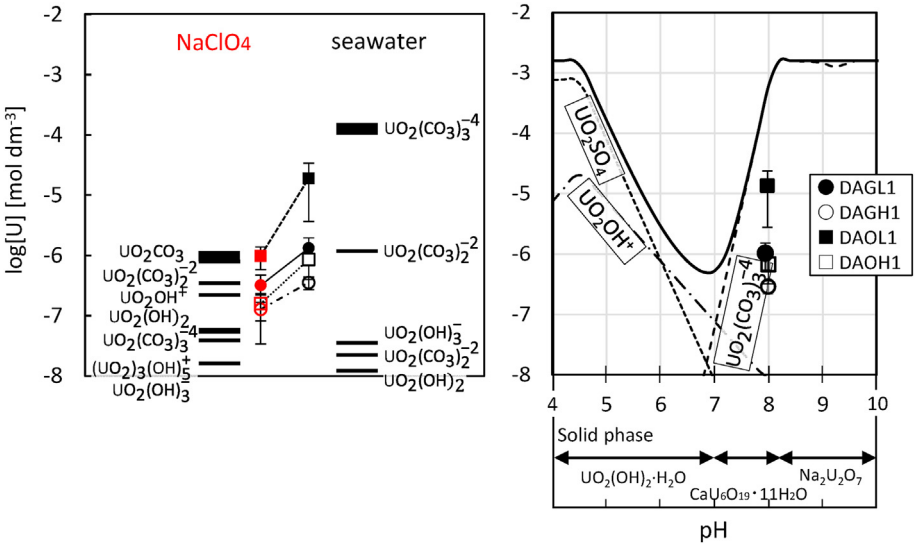

Fig. 5. Thermodynamic calculations of the solubility of U and experimental concentration of U after six months of immersion. U species in the samples immersed in a $NaClO_4$ solution ($I = 0.1$) and seawater (left). The detailed solution conditions are described in the text. pH dependence of the predominant species for the samples immersed in seawater (right). The calculation details are included in the text.

the solubility of uranyl in the seawater system was negligible. In summary, the solubility-limiting solid phases in the $NaClO_4$ systems were metaschoepite at pH < 7.5, $Na_2U_2O_7$ at pH > 7.5 [35], whereas those in the seawater systems were metaschoepite at pH < 7.0, bequerelite in the pH range of 7.0–8.2, and $Na_2U_2O_7$ at pH > 8.2. The experimental values for the concentration of U in the DAOL1 samples, which comprised mixtures of U_3O_8 and (Fe, Cr)UO_4, were comparable to the estimated solubility values. In contrast, the log[U] values of the DAGL1, DAGH1, and DAOH1 comprising UO_2 and/or (U, Zr)O_2 phases were approximately 0.5 times lower than those of the DAOL1, indicating that the dissolution of the simulated debris samples in water which equilibrium with air was suppressed. After six months of leaching, the log r_{Fe} values were low (as low than −4) and were independent of the samples and solution conditions (Fig. S8). In addition, the trends in log r_{Zr} values were similar to those in log r_{Fe} values, even though the primary solid phases were different, such as ZrO_2 or metal (Fig. S9). Thus far, it has been challenging to identify the cause for the suppression of the U dissolution using the chemical states of the coexisting Fe and Zr compounds.

3.3.4. Dissolution behavior of the FPs

Fig. 4 shows the r_M (M = Cs, Sr, Ba, Ru, and Eu) values of the samples in the D- and I-series prepared by heating at 1873 K under a 1 ppm O_2 and Ar + 4% H_2 atmosphere for 1 h followed by immersion in a $NaClO_4$ solution. The log r_{Cs} values of the samples in the D- and I-series were approximately 0, indicating that most cold Cs preferentially leached out after only one day of immersion. The log r_{Sr} values of the samples in the D-series were comparable to the log r_{Cs} values. Therefore, unlike U leaching, Cs and Sr leaching was independent of the SUS and Zr components. Moreover, the log r_{Ba} values for the samples in the I-series were approximately one order of magnitude lower than the log r_{Sr} values. The inventory of doped cold Sr would be approximately 10^5 times higher than that of ^{140}Ba as a fission product. As indicated by the elemental distributions obtained using SEM–EDX (Fig. S5), water-soluble Sr species, such as strontium oxide, co-existed independently of the distribution of U. However, the trace amounts of Ba present in the neutron-irradiated simulated debris samples were distributed homogeneously throughout the samples. The trace amounts of Ba produced via the fission reaction of ^{235}U in the simulated debris could have undergone local stabilization in the U compounds to form a type of solid solution. Furthermore, the dissolution behavior of Ba in the spent fuel of nuclear power plants may be different from that of Ba in the simulated debris samples in this study because Ba can be released from fuel or react with other materials and change the chemical composition of fuel under high-temperature conditions during meltdown [36].

The r_{Ru} values were lower than the r_{137Cs} and r_{140Ba} values for the samples in the I-series. Similar to r_U, r_{Ru} decreased in the presence of SUS and Zr, which agreed with previously reported results [13]. The trend in the r_{Eu} values of the samples in the D-series was similar to that of r_{Ru}, and the valence states of cold Eu and Ru in the aqueous phases of the samples in the D-series were III and IV, respectively [37,38]. Therefore, the dissolution behavior of Eu and Ru was similar to that of U, and leaching was suppressed in the presence of SUS and Zr, as revealed by the r_U values. In addition, a $Eu_yU_{1-y}O_{2+x}$ solid solution was formed via heating a mixture of UO_2 and Eu_2O_3 at 1673 K in vacuo [39]. A similar (U, Zr, Eu)O_2 solid solution could have formed in this study. Therefore, cold Eu doping of the samples can be used to evaluate the leaching of trivalent or higher valence nuclides.

4. Conclusion

The U in the solid samples synthesized using UO_2, Zr, and SUS formed different compounds depending on the oxygen potential during heating, temperature, and heating time. The UO_2 phase did not change upon heating at 1473 K under the low oxygen potential of a 1 ppm O_2 atmosphere; however, a (U, Zr)O_2 solid solution formed at 1873 K. Conversely, under a low O_2 atmosphere (2% O_2), a mixture of U_3O_8 and (Fe, Cr)UO_4 phases formed upon heating at 1473 K. The formation of a Fe–Zr alloy phase was also observed. These materials must be typical constituents of the fuel debris generated by the severe accident at the Fukushima Daiichi Nuclear Power Station. For units 1 and 2, for which the partial pressure of O_2 and oxygen potential were low, the formation of alloy phases and a (U, Zr)O_2 solid solution is expected under such a condition. U_3O_8 and (Fe, Cr)UO_4 phases may have formed during the oxidation of U and metals in unit 3.

The dissolution behavior of the FPs in the prepared simulated fuel debris samples was examined using methods similar to those employed in previous studies on UO_2 and UO_2–ZrO_2 solid solutions, and the results indicated that the dissolution of U in the (U, Zr)O_{2+x} phase was suppressed compared with that in the UO_2 phase. The dissolution of U also depended on the aqueous conditions. For the seawater system, the apparent U concentration increased over time because of the formation of soluble uranyl carbonate complex ions, whereas for the $NaClO_4$ system, the apparent U concentration remained almost constant. In contrast, the dissolution of oxidized U from mixtures of U_3O_8 and (Fe, Cr)UO_4 was promoted over that of UO_2. However, the U_3O_8-to-(Fe, Cr)UO_4 ratio did not affect the dissolution behavior of U. Therefore, further research is needed to clarify whether this phenomenon is due to differences in the dissolution properties of the two primary U components or to differences in other components such as iron oxide in the mixture.

Several findings on the dissolution behavior of the FPs in the simulated debris were also obtained. For example, Cs was preferentially dissolved over U regardless of the composition and properties of the synthesized solid phase, which was consistent with previously reported data. This supported the hypothesis that the gamma radioactivity of the contaminated water generated by the cooling of the Fukushima Daiichi Nuclear Power Station was high. In contrast, Sr and Ba leached regardless of the chemical compositions of the samples in the D- and I-series. Furthermore, the dissolution of Eu and Ru was suppressed because of their high valences, and the incorporation of Eu and Ru into the U compounds in the simulated debris and their harmonic dissolution via solid-solution reactions were observed.

Declaration of competing interest

The authors declare that they have no known competing financial interests or personal relationships that could have appeared to influence the work reported in this paper.

Acknowledgments

This work was supported by the JAEA Nuclear Energy S&T and Human Resource Development Project through concentrated wisdom, grant number JPJA18P18071886. The authors would like to acknowledge Dr. Shun Sekimoto and the staff at the Institute for Integrated Radiation and Nuclear Science, Kyoto University (KURNS), for their significant contributions to the experiments. The authors would also like to express their gratitude to the members of the research reactor group at KURNS for their help with the neutron irradiation experiments and for allowing us to use the KUR supported by Kyoto University.

Appendix A. Supplementary data

Supplementary data to this article can be found online at https://doi.org/10.1016/j.net.2022.12.017.

References

[1] Tokyo Electric Power Company, Evaluation of the Status of the Reactor Core Damage at the Fukushima Daiichi Nuclear Power Station Units 1–3, 2017. http://www.tepco.co.jp/press/release/2017/pdf2/171225j0102.pdf.
[2] Tokyo Electric Power Company, Situation of the Primary Containment Vessel Based on Gas Measurement Results, 2012. http://www.tepco.co.jp/nu/fukushima-np/images/handouts_120723_06-j.pdf.
[3] T. Sasaki, Y. Takeno, A. Kirishima, N. Sato, Leaching test of gamma-emitting Cs, Ru, Zr, and U from neutron-irradiated UO_2/ZrO_2 solid solutions in non-filtered surface seawater: Fukushima NPP Accident Related, J. Nucl. Sci. Technol. 52 (2015) 147–151.
[4] N. Sato, A. Krishima, T. Sasaki, Behavior of fuel and structural materials in severely damaged reactors, Adv. Sci. Technol. 94 (2014) 93–96.
[5] P. Piluso, G. Trillon, C. Journeau, The UO_2–ZrO_2 system at high temperature (T > 2000 K): importance of the meta-stable phases under severe accident conditions, J. Nucl. Mater. 344 (2005) 259–264.
[6] Yu.B. Petrov, Yu.P. Udalov, J. Subrt, S. Bakardjieva, P. Sazavsky, M. Kiselova, P. Selucky, P. Bezdicka, C. Journeau, P. Piluso, Phase equilibria during crystallization of melts in the uranium oxide-iron oxide system in air, Glass Phys. Chem. 35 (2009) 298–307.
[7] D. Akiyama, H. Akiyama, A. Uehara, A. Kirishima, N. Sato, Phase analysis of uranium oxides after reaction with stainless steel components and ZrO_2 at high temperature by XRD, XAFS, and SEM/EDX, J. Nucl. Mater. 520 (2019) 27–33.
[8] V.I. Almjashev, M. Barrachin, S. Bechta, D. Bottomley, S.A. Vitol, V.V. Gusarov, F. Defoort, E.V. Krushinov, D.B. Lopukh, A.V. Lysenko, A.P. Martynov, L.P. Mezentseva, A. Miassoedov, Yu.B. Petrov, M. Fischer, V.B. Khabensky, S. Hellmann, Ternary eutectics in the systems FeO-UO_2-ZrO_2 and Fe_2O_3-U_3O_8-ZrO_2, Radiochemistry 53 (2011) 13–18.
[9] Yu.B. Petrov, Y.P. Udalov, J. Subrt, S. Bakardjieva, P. Sazavsky, M. Kiselova, P. Selucky, P. Bezdicka, C. Journeau, P. Piluso, Experimental investigation and thermodynamic simulation of the uranium oxide–zirconium oxide–iron oxide system in air, Glass Phys. Chem. 37 (2011) 212–229.
[10] A. Kirishima, D. Akiyama, Y. Kumagai, R. Kusaka, M. Nakada, M. Watanabe, T. Sasaki, N. Sato, Structure, stability, and actinide leaching of simulated nuclear fuel debris synthesized from UO_2, Zr, and stainless-steel, J. Nucl. Mater. 567 (2022), 153842.
[11] Japanese Ministry of Economy Trade and Industry, Tokyo, Nuclear Accident Response Office, Agency for Natural Resources and Energy, Important Stories on Decommissioning 2018, Fukushima Daiichi Nuclear Power Station, Now and in the Future, 2018. https://www.meti.go.jp/english/earthquake/nuclear/decommissioning/pdf/20180827_roadmap.pdf.
[12] Industry JMoETa, Released Meeting Materials at Secretariat Meeting of the Team for Countermeasures for Decommissioning and Contaminated Water Treatment, 2019.
[13] T. Sasaki, Y. Takeno, T. Kobayashi, A. Kirishima, N. Sato, Leaching behavior of gamma-emitting fission products and Np from neutron-irradiated UO_2–ZrO_2 solid solutions in non-filtered surface seawater, J. Nucl. Sci. Technol. 53 (2016) 303–311.
[14] A. Kirishima, M. Hirano, T. Sasaki, N. Sato, Leaching of actinide elements from simulated fuel debris into seawater, J. Nucl. Sci. Technol. 52 (2015) 1240–1246.
[15] A. Kirishima, M. Hirano, D. Akiyama, T. Sasaki, N. Sato, Study on the leaching behavior of actinides from nuclear fuel debris, J. Nucl. Mater. 502 (2018) 169–176.
[16] T. Sasaki, S. Sakamoto, D. Akiyama, A. Kirishima, T. Kobayashi, N. Sato, Leaching behavior of gamma-emitting fission products, calcium, and uranium from simulated MCCI debris in water, J. Nucl. Sci. Technol. 56 (2019) 1092–1102.
[17] S. Gražulis, A. Daškevič, A. Merkys, D. Chateigner, L. Lutterotti, M. Quirós, N.R. Serebryanaya, P. Moeck, R.T. Downs, A. Le Bail, Crystallography Open Database (COD): an open-access collection of crystal structures and platform for world-wide collaboration, Nucleic Acids Res. 40 (2012) D420–D427.
[18] R. Young, A.C. Larson, C. Paiva-Santos, Rietveld Analysis of X-Ray and Neutron Powder Diffraction Patterns, School of Physics, Georgia Institute of Technology, Atlanta (GA), 1998.
[19] Y. Takaya, T. Nakayama, C. Oguchi, T. Hatta, Experimental study on alteration of mortars attacked by seawater–secondary products on surface, J. MMIJ 125 (2009) 489–495.
[20] Y. Ikeda, Y. Yasuike, K. Nishimura, S. Hasegawa, Y. Takashima, Kinetic study on dissolution of UO_2 powders in nitric acid, J. Nucl. Mater. 224 (1995) 266–272.
[21] F. Grønvold, High-temperature X-ray study of uranium oxides in the UO_2-U_3O_8 region, J. Inorg. Nucl. Chem. 1 (1955) 357–370.
[22] F. Stein, G. Sauthoff, M. Palm, Experimental determination of intermetallic phases, phase equilibria, and invariant reaction temperatures in the Fe-Zr system, J. Phase Equilibria 23 (2002) 480–494.
[23] P. Nash, C. Jayanth, The Ni– Zr (nickel-zirconium) system, Bull. Alloy Phase Diagrams 5 (1984) 144–148.
[24] E. Hayes, A. Roberson, M. Davies, Zirconium-chromium phase diagram, JOM 4 (1952) 304–306.
[25] L. Zhang, A. Shelyug, A. Navrotsky, Thermochemistry of UO_2–ThO_2 and UO_2–ZrO_2 fluorite solid solutions, J. Chem. Thermodyn. 114 (2017) 48–54.
[26] R. Ploc, The lattice parameter of cubic ZrO_2 formed on zirconium, J. Nucl. Mater. 99 (1981) 124–128.
[27] I. Cohen, B.E. Schaner, A metallographic and X-ray study of the UO_2-ZrO_2 system, J. Nucl. Mater. 9 (1963) 18–52.
[28] N.K. Kulkarni, K. Krishnan, U.M. Kasar, S.K. Rakshit, S.K. Sali, S.K. Aggarwal, Thermal studies on fluorite type $Zr_yU_{1-y}O_2$ solid solutions, J. Nucl. Mater. 384 (2009) 81–86.
[29] P. Evans, The system UO_2-ZrO_2, J. Am. Ceram. Soc. 43 (1960) 443–446.
[30] A. Uehara, D. Akiyama, A. Ikeda-Ohno, C. Numako, Y. Terada, K. Nitta, T. Ina, S. Takeda-Homma, A. Kirishima, N. Satob, Speciation on the reaction of uranium and zirconium oxides treated under oxidizing and reducing atmospheres, J. Nucl. Mater. 559 (2022), 153422.
[31] I. Grenthe, X. Gaona, L. Rao, A. Plyasunov, W. Runde, B. Grambow, R. Konings, A. Smith, E. Moore, M.-E. Ragoussi, J.S. Martinez, D. Costa, A. Felmy, K. Spahiu,

Second Update on the Chemical Thermodynamics of Uranium, Neptunium, Plutonium, americium and technetium Organisation for Economic Co-Operation and Development, Paris, 2020.
[32] C.F. Baes, R.S. Mesmer, The Hydrolysis of Cations, John Wiley & Sons, New York, London, Sydney, Toronto, 1976.
[33] R. Guillaumont, F.J. Mompean, Update on the Chemical Thermodynamics of Uranium, Neptunium, Plutonium, Americium and Technetium, Elsevier, Amsterdam, 2003.
[34] I. Grenthe, J. Fuger, R.J.M. Konings, R.J. Lemire, A.B. Muller, C. Nguyen-Trung, H. Wanner, Chemical Thermodynamics of Uranium, Elsevier, Amsterdam, 1992.
[35] M. Altmaier, E. Yalçıntaş, X. Gaona, V. Neck, R. Müller, M. Schlieker, T. Fanghänel, Solubility of U (VI) in chloride solutions. I. The stable oxides/hydroxides in NaCl systems, solubility products, hydrolysis constants and SIT coefficients, J. Chem. Thermodyn. 114 (2017) 2–13.
[36] W.E. Browning Jr., C.E. Miller, R.P. Shields Jr., B.F. Roberts, Release of fission products during in-pile melting of UO_2, Nucl. Sci. Eng. 18 (1964) 151–162.
[37] V.I. Paramonova, E.F. Latyshev, The ion exchange method in studies of the state of matter in solution. Vi. Complexing ruthenium (iv) in hydrochloric and perchloric acids, Radiokhimiya (1) (1959).
[38] M. Jiménez-Reyes, M. Solache-Ríos, A. Rojas-Hernández, Application of the specific ion interaction theory to the solubility product and first hydrolysis constant of europium, J. Solut. Chem. 35 (2006) 201–214.
[39] T. Fujino, K. Ouchi, Y. Mozumi, R. Ueda, H. Tagawa, Composition and oxygen potential of cubic fluorite-type solid solution $Eu_yU_{1-y}O_{2+x}$($x \gtrapprox 0$) and rhombohedral $Eu_6UO_{12+x'}$($x' < 0$), J. Nucl. Mater. 174 (1990) 92–101.